

## GENERAL ARTICLE

# BRCA1 mislocalization leads to aberrant DNA damage response in heterozygous ABRAXAS1 mutation carrier cells

Muthiah Bose<sup>1,†</sup>, Juliane Sachsenweger<sup>2,1</sup>, Niina Laurila<sup>1</sup>, Ann Christin Parplys<sup>3</sup>, Jonas Willmann<sup>3</sup>, Johannes Jungwirth<sup>4</sup>, Marco Groth<sup>5</sup>, Katrin Rapakko<sup>6</sup>, Pentti Nieminen<sup>7</sup>, Thomas W. P. Friedl<sup>2</sup>, Lisa Heiserich<sup>8</sup>, Felix Meyer<sup>3</sup>, Hanna Tuppurainen<sup>1</sup>, Hellevi Peltoketo<sup>1</sup>, Heli Nevanlinna<sup>9</sup>, Katri Pylkäs<sup>1</sup>, Kerstin Borgmann<sup>3</sup>, Lisa Wiesmüller<sup>2</sup>, Robert Winqvist<sup>1,\*</sup> and Helmut Pospiech<sup>4,10,\*</sup>

<sup>1</sup>Laboratory of Cancer Genetics and Tumor Biology, Cancer and Translational Medicine Research Unit, Biocenter Oulu, University of Oulu and NordLab Oulu, 90220 Oulu, Finland, <sup>2</sup>Department of Obstetrics and Gynecology, Ulm University, 89075 Ulm, Germany, <sup>3</sup>Laboratory of Radiobiology and Experimental Radiooncology, University Cancer Center Hamburg (UCCH), University Medical Center Hamburg-Eppendorf, 20246 Hamburg, Germany, <sup>4</sup>Project group Biochemistry, Leibniz Institute on Aging – Fritz Lipmann Institute, 07745 Jena, Germany, <sup>5</sup>Core Facility DNA Sequencing, Leibniz Institute on Aging–Fritz Lipmann Institute, 07745 Jena, Germany, <sup>6</sup>Laboratory of Genetics, Northern Finland Laboratory Centre NordLab Oulu, 90220 Oulu, Finland, <sup>7</sup>Department of Medical Informatics and Statistics, University of Oulu, 90220 Oulu, Finland, <sup>8</sup>Medipap GmbH, 15827 Dahlewitz/Berlin, Germany, <sup>9</sup>Department of Obstetrics and Gynecology, University of Helsinki and Helsinki University Central Hospital, Biomedicum Helsinki, 00029 Helsinki, Finland, and <sup>10</sup>Faculty of Biochemistry and Molecular Medicine, University of Oulu, 90220 Oulu, Finland

\*To whom correspondence should be addressed at: Leibniz Institute on Aging–Fritz Lipmann Institute, 07745 Jena, Germany; Faculty of Biochemistry and Molecular Medicine, University of Oulu, 90220 Oulu, Finland. Tel: +49-3641-656290; Email: helmut.pospiech@leibniz-fli.de or helmut.pospiech@oulu.fi and Laboratory of Cancer Genetics and Tumor Biology, University of Oulu and NordLab Oulu, 90220 Oulu, Finland. Tel: +358-400-476815; Email: robert.winqvist@oulu.fi

## Abstract

Whilst heterozygous germline mutations in the ABRAXAS1 gene have been associated with a hereditary predisposition to breast cancer, their effect on promoting tumourigenesis at the cellular level has not been explored. Here, we demonstrate in patient-derived cells that the Finnish ABRAXAS1 founder mutation (c.1082G > A, Arg361Gln), even in the heterozygous state leads to decreased BRCA1 protein levels as well as reduced nuclear localization and foci formation of BRCA1 and CtIP. This causes disturbances in basal BRCA1-A complex localization, which is reflected by a restraint in error-prone DNA

<sup>†</sup>Current address: Biotech Research & Innovation Centre, University of Copenhagen, 2200 Copenhagen, Denmark

Received: May 7, 2019. Revised: August 31, 2019. Accepted: September 2, 2019

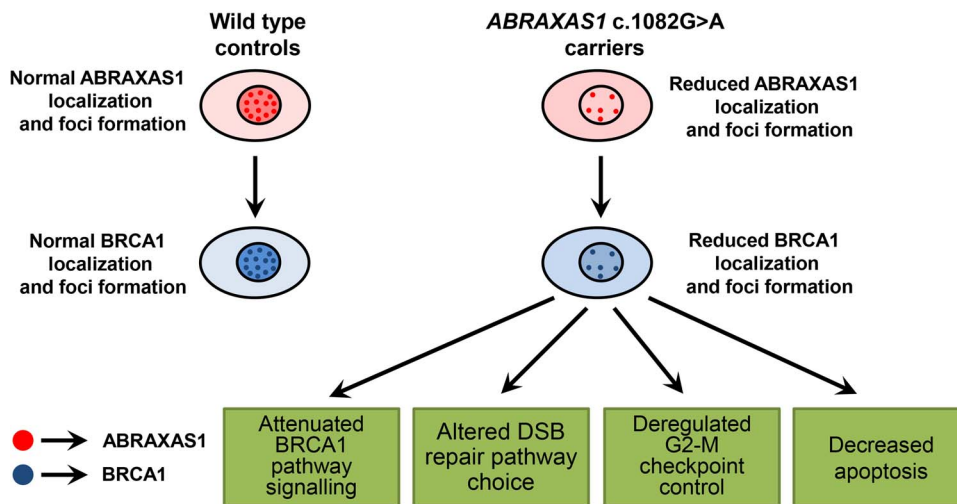
© The Author(s) 2019. Published by Oxford University Press.

This is an Open Access article distributed under the terms of the Creative Commons Attribution Non-Commercial License (<http://creativecommons.org/licenses/by-nc/4.0/>), which permits non-commercial re-use, distribution, and reproduction in any medium, provided the original work is properly cited. For commercial re-use, please contact [journals.permissions@oup.com](mailto:journals.permissions@oup.com)

double-strand break repair pathway usage, attenuated DNA damage response and deregulated G2-M checkpoint control. The current study clearly demonstrates how the Finnish *ABRAXAS1* founder mutation acts in a dominant-negative manner on *BRCA1* to promote genome destabilization in heterozygous carrier cells.

## Graphical Abstract

### Proposed model how an *ABRAXAS1* NLS mutation may drive cancer



## Introduction

*ABRAXAS1* (*BRCA1* A complex subunit *abraxas* 1, a.k.a. *ABRA1*, *CCDC98* or *FAM175A*) is a tumour-suppressor gene in the *BRCA* pathway that displays mutations or copy number loss in several human cancers (1). The gene encodes a protein of 409 amino acids (aa; 47 kDa), containing four recognized key elements: an Mpr1 and PAD1 N-terminal (MPN)-like domain (aa 11–121), a coiled-coil region (aa 206–260), a nuclear localization signal (NLS, aa 358–361) and a pSPxF motif (aa 406–409) (2).

*ABRAXAS1* acts as the central scaffold protein of the *BRCA1*-A complex, which is comprised of *BRCA1*, *ABRAXAS1*, *MERIT40*, *RAP80*, *BRCC45* and *BRCC36* (2–5). When phosphorylated at its pSPxF motif, *ABRAXAS1* is being bound by the C-terminal domain of *BRCA1* (BRCT) (2–4). The NLS domain is important for translocation of *BRCA1*-A complexes into the cell nucleus to DNA damage sites (6).

Upon histone H2AX phosphorylation at serine 139 ( $\gamma$ -H2AX), *RNF8* and *RNF168* are recruited to the DNA damage sites, which generates K63 linked poly-ubiquitin (Ub) chains on histones (7). These are bound by *RAP80* via its Ub interacting motif domains and thus act as docking sites for the *BRCA1*-A complex (8). It is suggested that this multiprotein complex regulates the DNA damage response process by deubiquitinating the K63-linked poly-Ub chains (5). Consequently, down-regulation of any component in the *BRCA1*-A complex compromises the recruitment of *BRCA1* to the DNA damage sites (2,9–14).

In addition to *ABRAXAS1*, the *BRCA1* BRCT domain also directly binds some other pSPxF motifs in a phosphorylation-dependent manner, thus enabling interaction with *BACH1*

(*BRIP1/FANCI*) and *CtIP* (*RBBP8*), resulting in the formation of *BRCA1*-B and *BRCA1*-C complexes, respectively (15). All three of these *BRCA1* containing complexes compete for the availability of the endogenous *BRCA1* protein. Disruption of the *BRCA1*-A complex by knockdown of *RAP80* or *ABRAXAS1* propagates *BRCA1*-B and *BRCA1*-C enhanced complex formation (8).

The *BRCA1*-A complex is also involved in G2-M checkpoint control, apoptosis and transcription (2,16). In 2012, we reported a heterozygous germline alteration, c.1082G > A (Arg361Gln), in the *ABRAXAS1* gene in Northern Finnish breast cancer (BC) families (6). Although hereditary cancer-associated mutations in *ABRAXAS1* in general appear to be relatively rare, c.1082G > A is a founder mutation in the Finnish population. According to the Exome Aggregation Consortium, the same mutation has also been observed in non-Finnish Europeans and Latinos (17). The specific alteration (Arg361Gln) resides in the NLS, and was shown in a model system to impair the localization of the *BRCA1*-A complex to the nucleus and ultimately interfering with the *BRCA1*-mediated DNA damage response (6). In addition, the *ABRAXAS1* NLS domain is frequently targeted by somatic missense mutations in several types of cancer (1).

In the current study, we have used peripheral blood samples and lymphoblastoid cell lines (LCLs) derived from heterozygous Finnish *ABRAXAS1* c.1082G > A (Arg361Gln) pathogenic variant carriers and ethnically as well as geographically matched healthy control individuals to study the molecular and biological mechanisms related to hereditary predisposition to BC. We demonstrate that in the heterozygous state the Finnish *ABRAXAS1* founder mutation leads to reduced protein levels as well as nuclear localization of *BRCA1*. This causes disturbances

in basal BRCA1-A complex localization, which is reflected by a restraint in error-prone DNA double-strand break (DSB) repair pathway usage, attenuated DNA damage response and leakiness of the G2-M checkpoint. Mislocalization of BRCA1 together with reduced BRCA1 (and BRCA1-A complex) mediated damage response provide a likely explanation for the cancer phenotypes observed in heterozygous Finnish ABRAXAS1 mutation carriers.

## Results

### Unchanged ABRAXAS1 expression level in heterozygous ABRAXAS1 c.1082G > A carrier cells

The Finnish ABRAXAS1 c.1082G > A founder mutation has been shown to be associated with increased risk and early onset of BC and possibly some other malignancies (6). Overexpression of ABRAXAS1 Arg361Gln was shown to affect BRCA1 foci formation (6), but it was unclear how this mutation affects cells at physiological levels in a heterozygous state. We therefore established a set of LCLs of ABRAXAS1 c.1082G > A carriers and geographically and ethnically matched controls. In quantitative polymerase chain reaction (qPCR) analysis, mutation carrier LCLs showed comparable ABRAXAS1 mRNA levels [ $96.8\% \pm 16.8\%$  (s.d.)] to those of controls (Supplementary Material, Fig. S1A). RNA-Seq data showed that ABRAXAS1 c.1082G > A transcripts were present at levels comparable to those of the wild-type (wt) allele ( $46.5\% \pm 6.7\%$  of total ABRAXAS1 reads including the c.1082 site; Supplementary Material, Table S1). In western blot (WB) analysis, we observed equal ABRAXAS1 protein expression in carrier and control cells (Supplementary Material, Fig. S1B and C), indicating that mutant ABRAXAS1 is endogenously expressed at the same level as and shows comparable stability to the wt protein (6,18).

### Mutant ABRAXAS1 protein causes partial BRCA1 mislocalization

Since the observed ABRAXAS1 single nucleotide change resides in the NLS domain responsible for nuclear localization, we investigated potential changes in its subcellular localization in our cohorts by using high content analysis. The automated analysis strategy used to assess the subcellular localization pattern of different proteins in a large number of cells unbiasedly is shown in Supplementary Material, Figure S2. As expected, we observed significantly less ABRAXAS1 localization in the nucleus of mutation carrier cells (z-scores, carriers:  $-1.97$  versus controls: 0.00,  $P = 0.0012$ ) (Fig. 1A). As BRCA1 constitutes a central part of the BRCA1-A complex, we also checked for the subcellular localization of BRCA1. Similarly to ABRAXAS1, there was a significantly smaller fraction of BRCA1 in the nucleus of ABRAXAS1 mutation carrier cells (z-scores, carriers:  $-2.12$  versus controls: 0.00,  $P = 0.0076$ ) (Fig. 1B). To confirm that expression of mutant ABRAXAS1 is sufficient for the mislocalization of BRCA1, we transiently transfected MCF7 cells with plasmids for expression of wt and c.1082G > A ABRAXAS1, respectively. Indeed, we observed a high correlation of BRCA1 subcellular misdistribution with that of recombinant mutant ABRAXAS1, but not with wt ABRAXAS1 (Supplementary Material, Fig. S3A). These results indicate that in ABRAXAS1 mutation carrier cells both ABRAXAS1 and BRCA1 proteins are to a significant degree mislocalized to the cytoplasm.

We next compared their foci formation pattern between our cohorts by automated high content analysis. In carrier cells, we observed 13.5% less spontaneous ABRAXAS1 foci, but

this remained under the statistical significance threshold (z-scores, carriers:  $-0.57$  versus controls: 0.00,  $P = 0.074$ ) (Fig. 1C and Supplementary Material, Fig. S3B). In parallel, the number of BRCA1 foci was significantly lower ( $\sim 55\%$  less; z-scores, carriers:  $-0.96$  versus controls: 0.00,  $P = 0.028$ ) in the ABRAXAS1 mutation carrier cells (Fig. 1D and Supplementary Material Fig. S3B). Furthermore, co-localization between ABRAXAS1 and BRCA1 foci was also significantly reduced in the ABRAXAS1 mutation carrier cells (co-localizing foci per nuclei, carriers: 0.83 versus controls: 2.13,  $P = 0.029$ ) (Fig. 1E). Importantly, the percentage of ABRAXAS1 foci coinciding with BRCA1, but not vice versa, was affected (Supplementary Material, Fig. S3C and D). The notion of reduced BRCA1-ABRAXAS1 complex formation in nuclei was supported by a proximity ligation assay (PLA), where the significant induction of ABRAXAS1 and BRCA1 interaction was no longer observed 4 h post irradiation (IR) in the ABRAXAS1 mutation carrier cells (Fig. 1F and G). Taken together, the results from both the current study using heterozygous mutation ABRAXAS1 mutation carrier cells and previous one (6) utilizing a cellular model system stably expressing this mutant allele support the view that the mutant ABRAXAS1 protein leads to reduced nuclear BRCA1-A complex localization.

### Reduced CtIP recruitment in cells from ABRAXAS1 mutation carriers

CtIP is a nuclease essential for activation of the microhomology-mediated end joining (MMEJ), single-strand annealing (SSA) and homologous recombination (HR) pathways (19). When inspecting the subcellular localization of CtIP, we found that similarly to both ABRAXAS1 and BRCA1, CtIP showed augmented localization to the cytoplasm relative to the nucleus in the heterozygous ABRAXAS1 mutation carrier cells (z-scores, carriers:  $-1.12$  versus controls: 0.00,  $P = 0.021$ ) (Fig. 2A). The cytoplasmic mislocalization of CtIP could also be reproduced by transient transfection of MCF7 cells with a plasmid expressing ABRAXAS1 c.1082G > A, but not the wt cDNA (Supplementary Material, Fig. S4A). Furthermore, the number of spontaneous CtIP foci was reduced by 35.5% (z-scores, carriers:  $-1.17$  versus controls: 0.00,  $P = 0.021$ ) in the mutation carrier cells (Fig. 2B). In WB, no significant change in CtIP expression between our cohorts was observed, indicating that CtIP mislocalization and its compromised recruitment is not due to differences in protein dosage (Supplementary Material, Fig. S4B,C).

Taken together, ABRAXAS1 mutation carriers display reduced levels of CtIP in the nucleus and thereby reduced recruitment to spontaneous DNA damage sites. The compromised CtIP recruitment is likely due to impaired recruitment of BRCA1, similarly to that found by Pathania and coworkers (20) in their study of BRCA1<sup>mut/+</sup> cells.

As S/G2 phase-specific phosphorylation of CtIP at Ser327 by CDKs is necessary for its interaction with BRCA1 and formation of the BRCA1-C complex (21), we checked for the levels of CtIPpSer327 in our two cohorts. In WB analysis, no significant change in CtIPpSer327 levels was observed between our cohorts (Supplementary Material, Fig. S4D-F). Moreover, PLA experiments also showed comparable association of BRCA1 and MRE11 at both untreated state and 4 h post IR in both cohorts (Supplementary Material, Fig. S4G), indicating no defects in BRCA1-C complex formation *per se*.

In respect to BRCA1-B complex formation, BACH1 and TopBP1 protein expression was potentially increased by 64 ( $P = 0.059$ ) and 71% ( $P = 0.058$ ), respectively, in our ABRAXAS1 mutation carrier cohort (Supplementary Material, Fig. S5A-D). However,

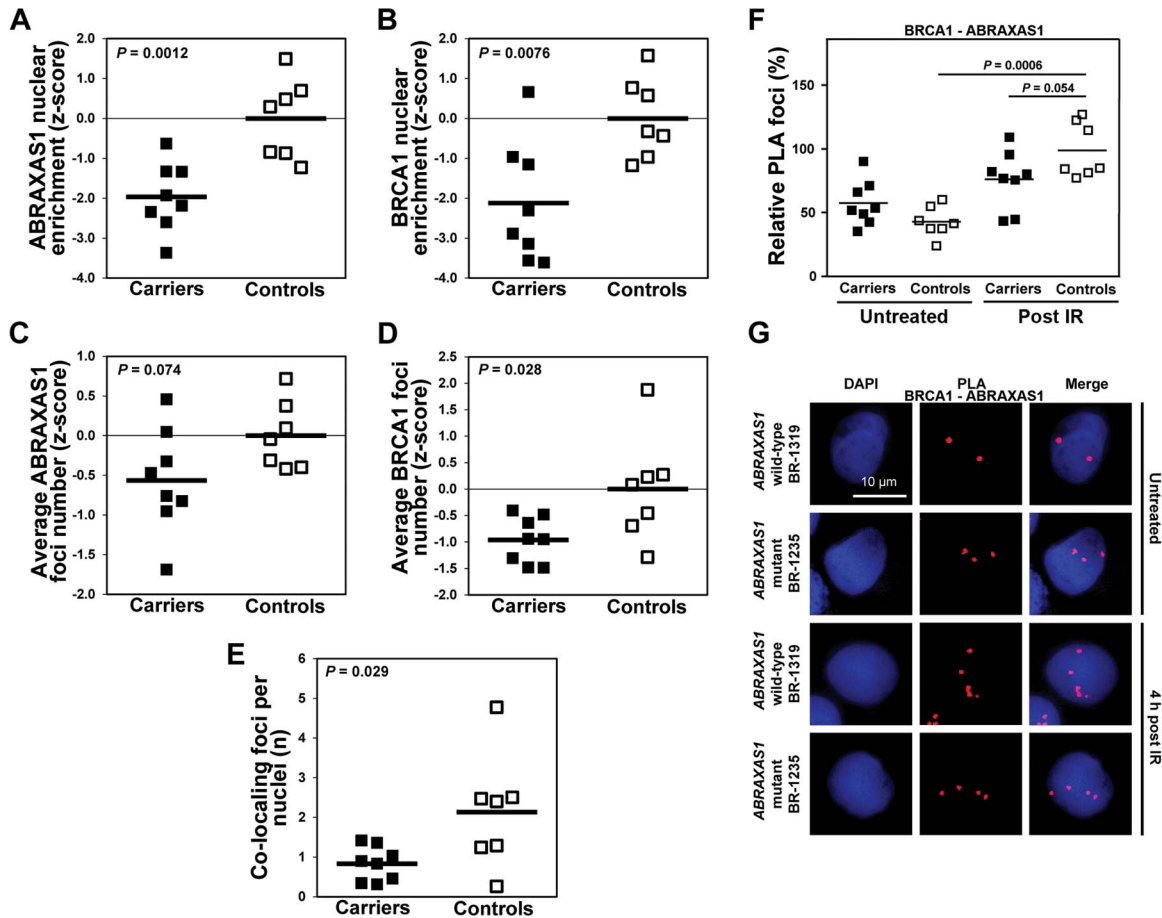


Figure 1. Mutant ABRAXAS1 protein affects the localization of BRCA1. Heterozygous ABRAXAS1 c.1082G > A mutation carrier LCLs show reduced relative nuclear localization of ABRAXAS1 (A) and BRCA1 (B) during unperturbed growth when compared to controls. The ratio between mean nuclear and cytoplasmic ABRAXAS1 and BRCA1 immunofluorescence signal intensity was determined utilising a high content analysis as described in [Supplementary Material, Figure S2](#). Furthermore, the mutation carriers show (C) a trend of lower average number of spontaneous ABRAXAS1 foci and (D) a significantly lower spontaneous BRCA1 foci number. In order to omit any bias derived from the use of specific fluorophores, biological repeats were performed with secondary antibodies conjugated with either AF488 or AF647. This affected the absolute numbers of foci detected per nuclei by the automated system, but not the relative abundance. Therefore, z-scores rather than foci numbers were averaged and statistically evaluated. For instance, using AF647 conjugates, we detected on average 4.42 foci per nucleus in ABRAXAS1 mutation carriers compared to 5.25 in controls. Also (E) a significant decrease in the number of co-localization between ABRAXAS1 and BRCA1 foci was observed in the mutation carriers. Lines in the dot plots (A–E) represent means and statistical significance was evaluated by two-tailed Student's t-test. Dot plot represent results from (A) six biological duplicates (BD); >3500 nuclei/sample analysed, (B) three BD; >2500 nuclei/sample, (C) four BD; >250 nuclei/sample and (D and E) > 50 nuclei/sample (single determination). Shown in (F and G) are the PLA findings for BRCA1 and ABRAXAS1. In (F) the mean values for irradiated controls were defined as 100% (absolute mean values are 5.2 foci/cell; two independent experiments). Statistically significant differences were calculated using Mann-Whitney U, two-tailed test. In (G) representative images of wt (BR-1319) and ABRAXAS1 mutant LCLs (BR-1235) are shown.

PLA experiments did not indicate any change in the interaction between BRCA1 and TopBP1 between our cohorts ([Supplementary Material, Fig. S5E](#)), suggesting that BRCA1-B complex formation was not affected.

### Impairment of BRCA1-A complex affects DNA repair pathway choice

Several studies have shown that the BRCA1-A complex is crucial for DSB signalling. In the light of reduced ABRAXAS1, BRCA1 and CtIP foci formation and complex localization to spontaneous DNA damage sites (Figs 1C–E and 2B and [Supplementary Material, Fig. S3C and D](#)) in the studied ABRAXAS1 mutation carrier cells, we set out to assess how this affects DSB repair pathway usage. We introduced different eGFP-based reporter constructs for total non-homologous end joining (NHEJ), HR, MMEJ, SSA and SSA + HR into the LCLs, followed by flow cytometric scoring of repair proficient eGFP positive cells (22,23). No significant

differences were observed in either NHEJ or HR repair pathway usage between the two cohorts (Fig. 3A and B). However, in the ABRAXAS1 mutation carrier cells we observed a significant decrease in the usage of error prone repair pathways: MMEJ (relative mean value in carriers: 61%,  $P = 0.001$ ), SSA (relative mean value in carriers: 86%,  $P = 0.029$ ) and SSA + HR (relative mean value in carriers: 76%,  $P = 0.004$ ) (Fig. 3C–E). These results indicate that activation of DSB repair pathways, which utilize excessive nucleolytic end trimming such as SSA and MMEJ are suppressed in ABRAXAS1 mutation carrier cells. Importantly, this is not due to increased population of cells in G1 phase in carrier cells, when NHEJ is favoured ([Supplementary Material, Fig. S6A, left panel \(0 h\)](#)).

Detection of single-stranded DNA by RPA and its subsequent phosphorylation by checkpoint kinases is a common indicator for end-resection. We observed a trend of reduced foci formation 4 h after IR with 2 Gy IR ( $P = 0.072$ ) by immunofluorescence microscopy analysis ([Supplementary Material, Fig. S7A](#)). On the

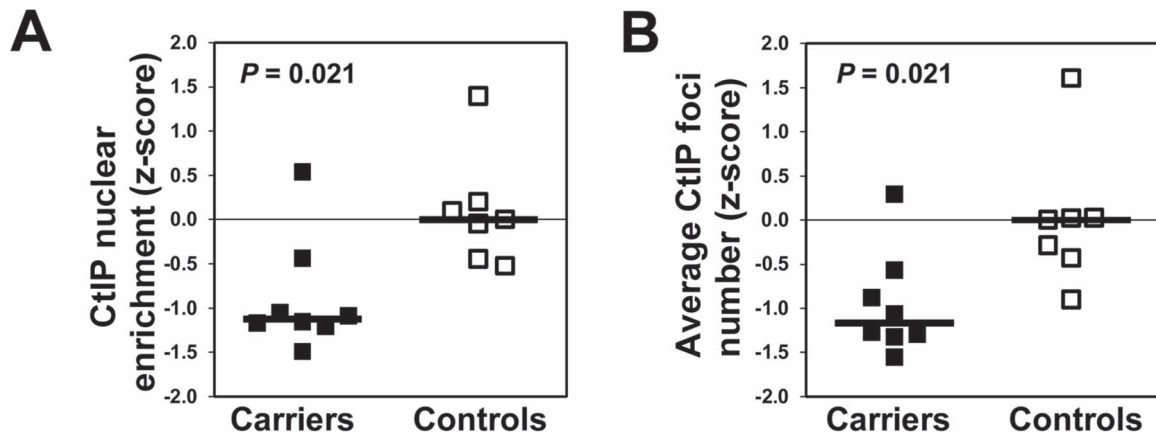


Figure 2. Heterozygous *ABRAXAS1* mutation affects CtIP localization. Heterozygous *ABRAXAS1* mutation carriers show (A) reduced relative nuclear localization of CtIP and (B) significantly less spontaneous CtIP foci during unperturbed growth than controls. Lines in the dot plot represent median, statistical significance of differences was evaluated by Mann–Whitney U test. Dot plot represent results from (A) two biological duplicates (BD); >1000 nuclei/sample analysed and (B) two BD; >150 nuclei/sample.

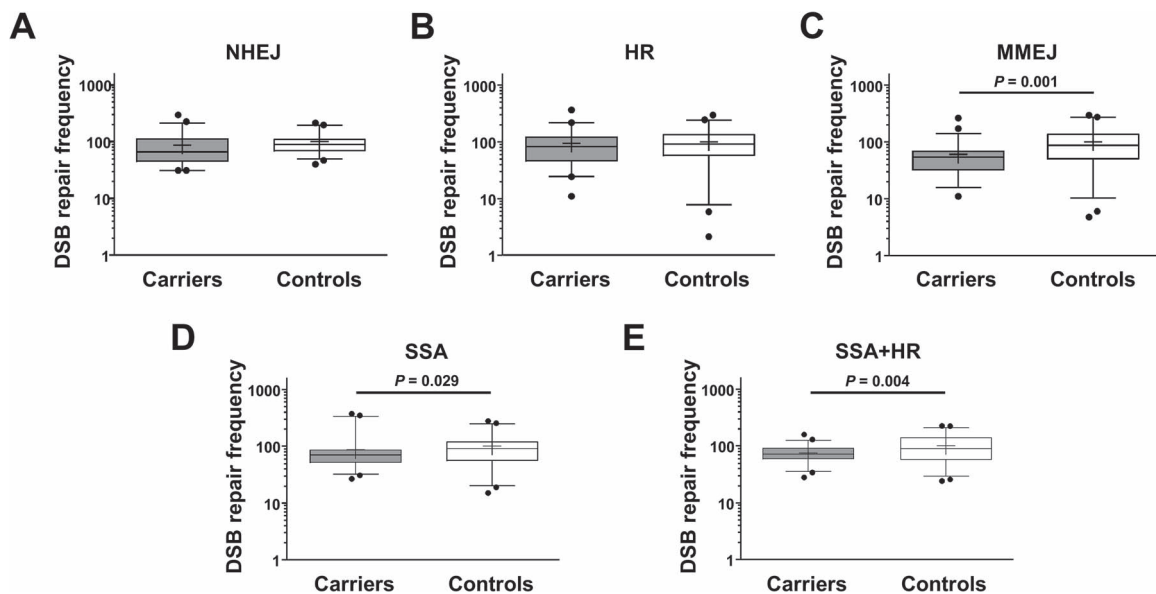


Figure 3. DSB repair pathway usage in heterozygous *ABRAXAS1*-mutated and wt individuals. Cohort analysis using a GFP reporter assay for the analysis of (A) NHEJ, (B) HR, (C) MMEJ, (D) SSA and (E) SSA + HR. LCLs from eight *ABRAXAS1* c.1082G > A mutation carriers (grey boxes) and seven wt *ABRAXAS1* individuals (white boxes) were transfected with reporter constructs for analysis as described in (20). From each LCL, six biological replicates were analysed in two independent experiments and normalized to the mean repair frequencies of all wt cell lines measured the same day, which was defined as 100% (average of absolute values corresponding to 100%: NHEJ,  $5.3 \times 10^{-3}$ ; HR,  $1.8 \times 10^{-4}$ ; MMEJ,  $3.3 \times 10^{-4}$ ; SSA,  $2.6 \times 10^{-3}$ ; SSA + HR,  $1.8 \times 10^{-3}$ ). Data are shown in box plots ( $n = 48$ ) including mean value (cross) and median (line), 95% CI. Statistically significant differences were calculated with SPSS using a general linear mixed model with mutation status as fixed factor and date of experiment as random factor.

other hand, when studying levels of RPA phosphorylated at Ser33 by flow cytometry before and after treatment with etoposide (ETO), there was no difference between carriers and controls in any cell cycle phase (Supplementary Material, Fig. S7B). We noticed that variation in phospho-RPA levels between different LCLs was high. Taken together, our data hint towards a reduced end resection, but do not support a major defect in end resection.

#### Heterozygously mutant *ABRAXAS1* cell lines display only marginally increased origin firing

Previously, we showed that LCLs of heterozygous carriers of the *PALB2* c.1592delT Finnish founder mutation displayed increased

dormant origin firing (24), and replication stress has been generally recognized as a major driver of genomic instability promoting tumourigenesis (25,26). We therefore studied DNA replication in a randomly selected subset of our *ABRAXAS1* mutation cohort using the DNA fibre assay. There is no apparent change in the elongation rate between our cohorts (Fig. 4A). Nevertheless, we observed a possible increase in the frequency of first pulse replication origins fired (carriers 17.7% versus controls 11.9%,  $P = 0.055$ ) in the *ABRAXAS1* mutation carrier cells (Fig. 4B). Unlike *PALB2* mutation carriers, we did not observe differences in the level of stalled forks after ETO treatment (Fig. 4C). It was previously suggested that *ABRAXAS1* is not required during replication as no changes were observed in stalled replication forks in *ABRAXAS1* knockout mouse embryonic fibroblasts (MEFs) (1). In the current study of heterozygous *ABRAXAS1* mutation carrier

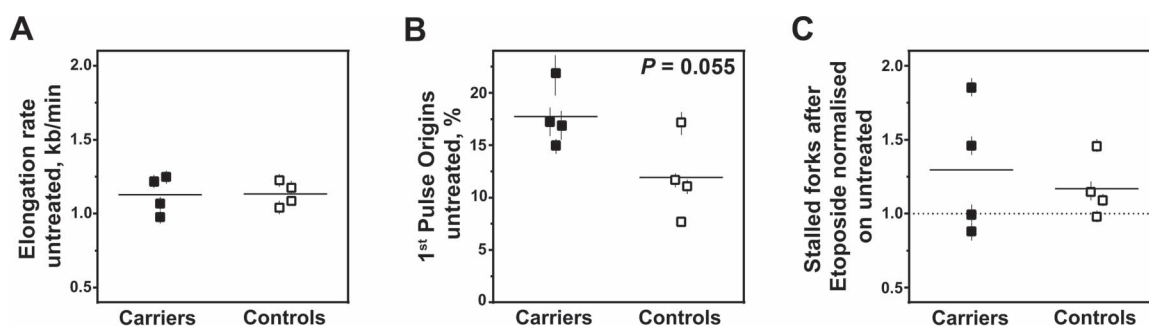


Figure 4. ABRAxAS1 mutation carrier cells display little DNA replication stress phenotype. DNA fibre assay showing changes in stalled forks, replication origin firing and elongation in four different ABRAxAS1 mutation carriers and four control cell lines. (A) Dot plot showing that there are no significant differences in elongation rate (kb/min) between our cohorts under normal growth conditions without any toxic treatment. However, (B) mutation carriers showed an increase in the frequency of first pulse replication origins fired. (C) Dot plot showing that there is no significant difference in the number of stalled forks present after ETO treatment between our cohorts. Stalled forks present after ETO treatment was normalized to the amount of stalled forks present in untreated conditions. Dot plot represent mean values  $\pm$  s.e.m. for each cell line. Lines in the dot plot represent means statistical significance of differences was evaluated by two-tailed Student's t-test. Dot plot represent results from >200 replication structures total from three independent determinations.

cells, however, the observance of a moderate increase in the first pulse replication origins fired could be attributed to the limited availability of BRCA1 as it is needed to support DNA replication particularly when experiencing stress (27).

When looking at spontaneous chromosomal aberrations, we did not observe any telomeric associations, complex chromosomal rearrangements, chromatid/chromosome breaks and deletions in primary lymphocytes of ABRAxAS1 mutation carriers (Supplementary Material, Table S2). There was, however, a possible slight increase in simple chromosomal rearrangements (carriers: 2.9 (0.0–4.0), controls: 0.0 (0.0–2.0),  $P = 0.108$ ) in the ABRAxAS1 mutation carrier cells (Supplementary Material, Table S2), but limitations in the availability of study material precluded conclusive evaluation. Taken together, ABRAxAS1 mutation carrier cells display only a moderate increase in origin firing replication phenotype, and at best, weak indications of chromosomal instability. This suggests that the cellular phenotypes observed in the mutation carrier LCLs are not primarily driven by DNA replication stress.

#### Attenuated G2-M checkpoint maintenance in ABRAxAS1 mutation carrier cells

As BRCA1-A is implicated in the DNA damage response, particularly G2-M checkpoint control, we next analysed cell cycle distribution in our cohorts in response to 0.5  $\mu$ M of the topoisomerase II inhibitor ETO. No significant change in cell cycle distribution was observed between our cohorts during the first 7 h of treatment (Supplementary Material, Fig. S6A and B). However, there was a significantly higher M/G2 ratio in the ABRAxAS1 mutation carriers at 24 h post ETO treatment, (relative M-G2 ratio in carriers—151%,  $P = 0.031$ ), which is indicative of G2-M checkpoint leakage (Fig. 5A). When following the response to ETO over time, it becomes apparent that both cohorts display a progressive G2 arrest, but mutation carrier cells to a lesser extent (Supplementary Material, Fig. S6B). This is in line with the observance of G2-M checkpoint failure after  $\gamma$ -IR in cells overexpressing mutant ABRAxAS1 protein (6). Thus, heterozygous ABRAxAS1 mutation carrier cells could activate the G2-M checkpoint proficiently, but maintained it less efficiently than the controls.

Both ataxia telangiectasia mutated (ATM) and CHK2 play a key role in activating and maintaining the G2-M checkpoint.

We therefore characterized the response of our cohorts to ETO treatment in terms of changes in ATM and CHK2 levels and phosphorylation. No significant change in the stabilisation and phosphorylation of ATM and CHK2 was observed between our cohorts during the first 7 h of treatment (Supplementary Material, Fig. S6C). However, at 24 h post ETO, we found significantly reduced ATM (79%,  $P = 0.019$ ) and CHK2 protein (72%,  $P = 0.031$ ) in ABRAxAS1 mutation carrier LCLs (Fig. 5B–E). Despite the presence of ATM damage response among mutation carriers, this reduced ATM and CHK2 levels at 24 h may explain the observed attenuation of G2-M checkpoint maintenance (28,29).

#### DNA damage persistence in heterozygous ABRAxAS1 mutation carrier cells

In order to address how the observed molecular phenotypes in our ABRAxAS1 LCL cohort influence the overall levels and progression of DNA damage and damage signalling, we investigated  $\gamma$ H2AX as an early global indicator of DSBs. At untreated state, no significant differences were seen in the spontaneous  $\gamma$ H2AX foci numbers between our cohorts (Supplementary Material, Fig. S8A). Instead, a moderate, nevertheless significant decrease in  $\gamma$ H2AX foci intensity by  $\sim 15.5\%$  was observed in the ABRAxAS1 mutation carrier cells (z-scores, carriers:  $-2.44$  versus controls: 0.00,  $P = 0.0024$ ) (Fig. 6A). To further elaborate on this observation, we used a flow cytometric approach to quantify global  $\gamma$ H2AX levels. Indeed, the ABRAxAS1 mutation carrier cells showed also a modest, but significant decrease in  $\gamma$ H2AX intensity (relative mean intensity in carriers: 90.4%,  $P = 0.031$ ) (Fig. 6B). When applying cell cycle specific analysis, we found a significant decrease in  $\gamma$ H2AX intensity only in the G1 (relative mean intensity, carriers: 89.8%,  $P = 0.021$ ) and S (relative mean intensity in carriers: 90.1%,  $P = 0.042$ ) (Fig. 6C) populations.

We next looked at the levels and persistence of DNA damage induced by ETO. There was no difference between the cohorts in foci numbers of 53BP1,  $\gamma$ H2AX and RAD51 in untreated condition or up to 7 h of treatment (Supplementary Material, Fig. S8). In contrast, at 24 h post ETO we found significantly increased numbers of 53BP1 ( $\sim 71\%$  more; z-scores, carriers: 3.48 versus controls: 0.00,  $P = 0.011$ ),  $\gamma$ H2AX ( $\sim 31\%$  more; z-scores, carriers: 1.66 versus controls: 0.00,  $P = 0.030$ ) and RAD51 foci ( $\sim 64\%$  more; z-scores, carriers: 2.14 versus controls: 0.00,  $P = 0.010$ ) in the mutation carrier cells, indicating the presence of more residual

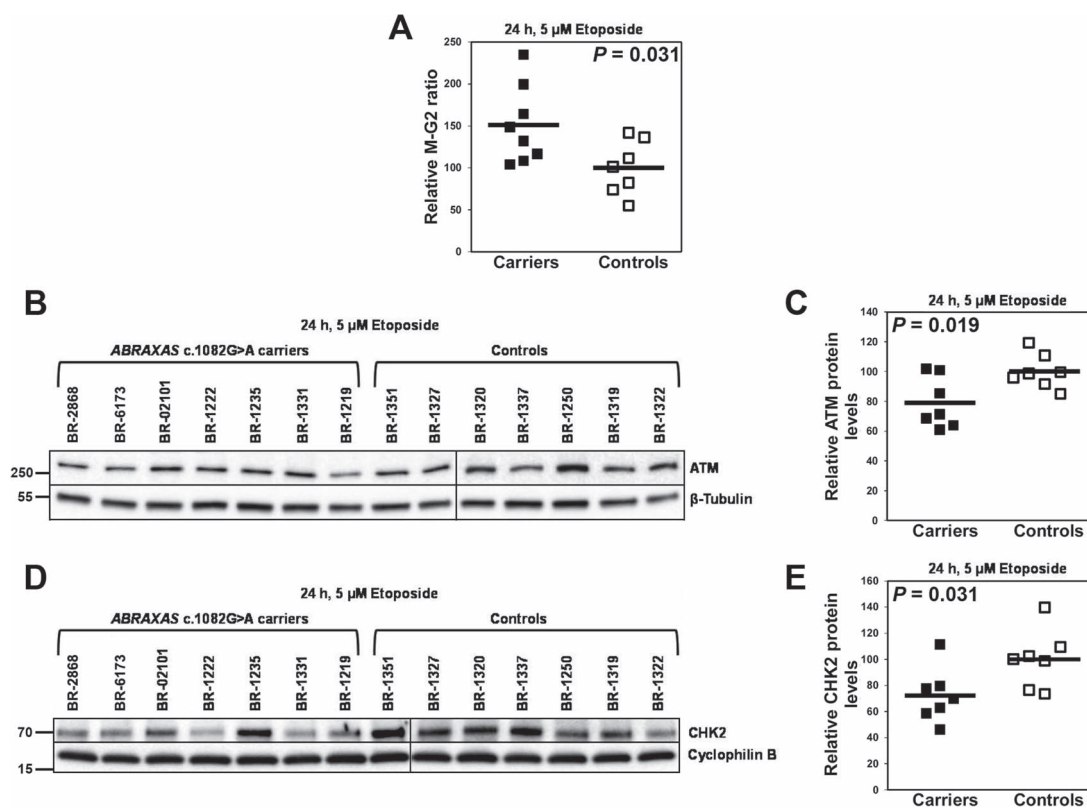


Figure 5. ABRAXAS1 mutation carriers show mild ATM checkpoint maintenance defect. (A) ABRAXAS1 mutation carriers show significantly more mitotic cells relative to G2 cells in presence of 0.5  $\mu$ M ETO for 24 h when compared to controls. G2-M checkpoint was analysed by flow cytometry, the mean M/G2 ratio of carriers was set to 100% for the controls in individual experiments. (B and D) Representative immunoblot showing ATM (B; 350 kDa) and CHK2 (D; 61 kDa) protein levels after 24 h presence of 5  $\mu$ M ETO. Protein levels were normalized against  $\beta$ -tubulin (55 kDa) and Cyclophilin B (21 kDa), respectively. Significant down-regulation of ATM (C) and CHK2 (E) was observed in ABRAXAS1 mutation carriers. Lines in the dot plot represent means; statistical significance of differences was evaluated by two-tailed Student's *t*-test. Dot plot represent results from (A) two biological duplicates; >20 000 events/sample analysed and (C and E) two technical repeats.

DNA damage (Fig. 7A–C). These results indicate that heterozygous ABRAXAS1 mutation carrier cells initiate DNA repair after ETO treatment with normal kinetics, but are left with more residual DNA damage at 24 h. This was not accompanied by a higher sensitivity of the carrier cells against DNA damage induced by ETO or MMC, as  $IC_{50}$  values determined by an alamarBlue assay for these agents did not differ significantly between carrier and control cell cohorts (Supplementary Material, Fig. S9). Previously, homozygous ABRAXAS1 knockout MEFs have shown high levels of unrepaired DNA damage after IR (1). Here we demonstrate a similar, albeit weaker phenotype in the heterozygous ABRAXAS1 mutation carrier cells.

We now analysed the response of ABRAXAS1, BRCA1 and CtIP after ETO treatment. Surprisingly, in contrast to the untreated state (Figs 1 and 2), no difference between the cohorts was observed in the subnuclear localization of ABRAXAS1, BRCA1 and CtIP after 7 h and 24 h of ETO treatment (Supplementary Material, Fig. S10A–F). All of these proteins were predominantly nuclear, indicating their engagement in repair of ETO-induced DNA damage. Similarly, all three proteins formed comparable numbers of foci in both cohorts at 7 h ETO (Supplementary Material, Fig. S10G–I). However, at 24 h of ETO, there was a potential increase in the number of foci formed by BRCA1 (~80% more; z-scores, carriers: 2.18 versus controls: 0.00,  $P = 0.068$ ) and CtIP (~27% more; z-scores, carriers: 0.86 versus controls: 0.00,  $P = 0.068$ ), but not by ABRAXAS1 in the mutation carrier cells (Fig. 7D–F). This is in line with the augmented level of RAD51 foci in the mutation carrier cells (Fig. 7C). It was previously

shown that BRCA1 is required for the recruitment of CtIP and RAD51 to the sites of DNA damage (20). Thus, all of the results are consistent with a delayed completion of DSB repair in the heterozygous ABRAXAS1 mutation carrier cells.

### Reduced caspase activation in heterozygous ABRAXAS1 mutation carrier cells

Recently, a pro-apoptotic role has been reported for the BRCA1-A complex (16). We therefore explored apoptosis activation by measuring flow cytometric caspase activation of our cohorts at both untreated state and after 24 h in the presence of 0.5  $\mu$ M ETO. In untreated ABRAXAS1 mutation carrier cells, there were significantly less caspase positive cells (9.4% and 13.1% of cells with active caspase in carriers versus control, respectively,  $P = 0.0052$ ; Fig. 8A). However, at 24 h of ETO treatment, we no longer observed any differences in the number of caspase positive cells between our cohorts (Fig. 8B).

### Discussion

Since the identification of BRCA1 and BRCA2 as high-risk BC susceptibility genes, it has become apparent that pathogenic variants in multiple genes of the BRCA damage response pathway increase the hereditary risk of BC and other malignancies. Functional characterisation of BC promoting mutations has traditionally been based on analysis of tumour-derived cell lines,

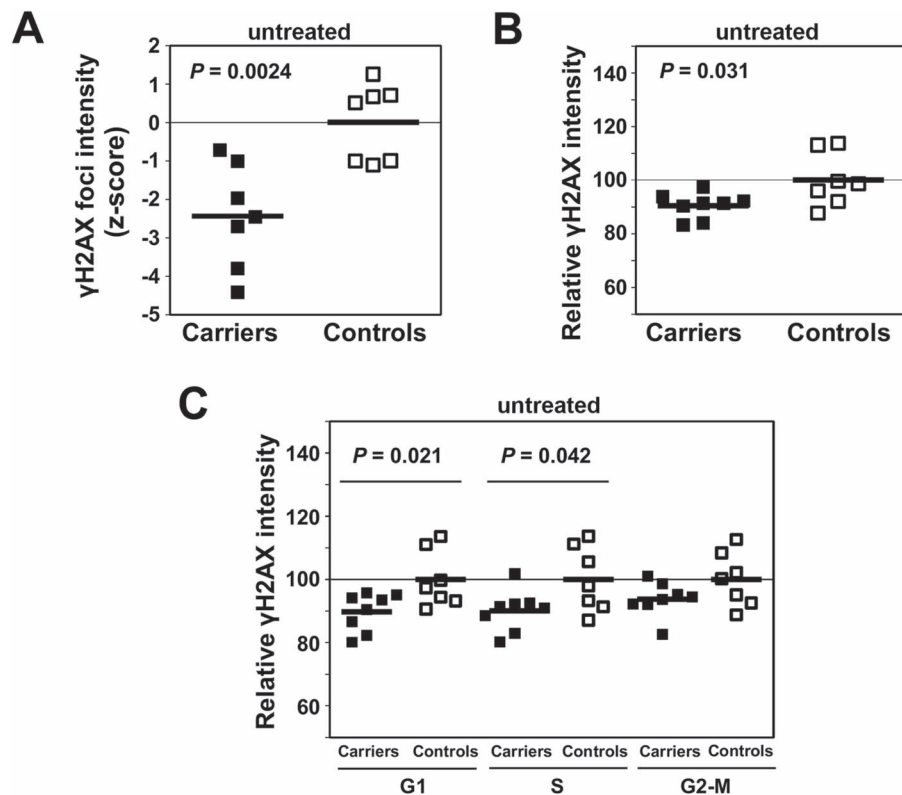


Figure 6. Heterozygous ABRAXAS1 mutation affects  $\gamma$ H2AX signalling. (A) ABRAXAS1 mutation carriers show significantly lower  $\gamma$ H2AX foci intensity than controls. Dots represent mean spontaneous  $\gamma$ H2AX foci intensity of individual LCLs during undisturbed growth. Averages of z-scores were used to accommodate for variation in absolute intensities between biological replicates. (B) Significantly reduced  $\gamma$ H2AX intensity in the whole cell population of ABRAXAS1 mutation carriers. (C)  $\gamma$ H2AX intensity is significantly lower only in G1 and S but not in the G2-M population of the mutation carriers. Lines in the dot plot represent means; statistical significance of differences was evaluated by two-tailed Student's t-test. Dot plot represent results from (A) three biological duplicates (BD); >50 nuclei/sample analysed, (B and C) three BD; >30 000 events/sample.

permanently or transiently induced mutant allele overexpression, cellular knockdown or knockout approaches or mouse models. Only few studies have taken on the challenge of analysing the molecular and biological effects of mutations at the heterozygous state, using patient-derived material or models. This may be due to the heterogeneity or limited availability of human samples and the less pronounced or recessive phenotypes found in the heterozygous state. However, increasing evidence points to subtle haplo-insufficiency (or possibly mild dominant-negative) phenotypes of BC susceptibility gene germline mutations (20,24,30) that likely represent important disease drivers early in tumorigenesis, alone or in combination with other acquired mutations (31–33).

In the present study, we have comprehensively characterized the molecular and functional consequences of the heterozygous Finnish ABRAXAS1 c.1082G > A founder mutation in a carrier-derived LCL cohort. Germline mutations in ABRAXAS1 have been associated with BC as well as certain types of rare cancers (6,34–36). The average age of disease onset for the Finnish ABRAXAS1 c.1082G > A mutation carriers is 51 years (variation: 35 to 60 years; this cohort), compared to 46 years in Finnish BRCA1 (variation: 32 to 57 years), 48 years in BRCA2 (variation: 45 to 67 years) and 53 years in PALB2 carriers (variation: 39 to 73 years) (37,38).

Our data support a model where attenuation of BRCA1-A function and reduced BRCA1 availability give rise to an aberrant DNA damage response that may be underlying the increased cancer susceptibility (Fig. 9).

From our results, it is apparent that the BRCA1 mislocalization is due to a dominant-negative effect of mutant ABRAXAS1 as shown in both LCLs and MCF7 cells. BRCA1 mislocalization in the ABRAXAS1 mutation carrier cells could also be directly responsible for the mislocalization of CtIP and subsequently MMEJ and SSA suppression in the carrier cells, likely due to reduced nuclear BRCA1-A complex formation (39). Alternatively, the overall balance between BRCA1-A, -B and -C complexes may be disturbed. Furthermore, our results suggest that the mislocalization and reduced levels of BRCA1 is the reason for attenuated G2-M checkpoint maintenance, higher DNA damage persistence and reduced caspase activation (Fig. 9).

It is noteworthy that most of the phenotypic changes observed in the ABRAXAS1 mutation carrier cells are mild in nature, as there are only moderate changes in ABRAXAS/BRCA1 expression and redistribution. It appears that only a subset of BRCA1 functions, directly or indirectly linked to the BRCA1-A complex have been significantly affected in the ABRAXAS1 mutation carriers. The changes observed in spontaneous formation of ABRAXAS1, BRCA1 and CtIP foci as well as persistence of DNA damage after ETO are likely due to attenuated DSB damage response signalling as well as reduced initiation of resection (40).

Beside the occurrence of specific ABRAXAS1 germline mutations affecting the NLS domain, the NLS of ABRAXAS1 has been identified as a mutational 'hot spot' in several types of tumours (1), suggesting that also somatic missense mutations disrupting the NLS are biologically relevant and may thus represent a driver of sporadic cancers. Furthermore, the observed mutational 'hot

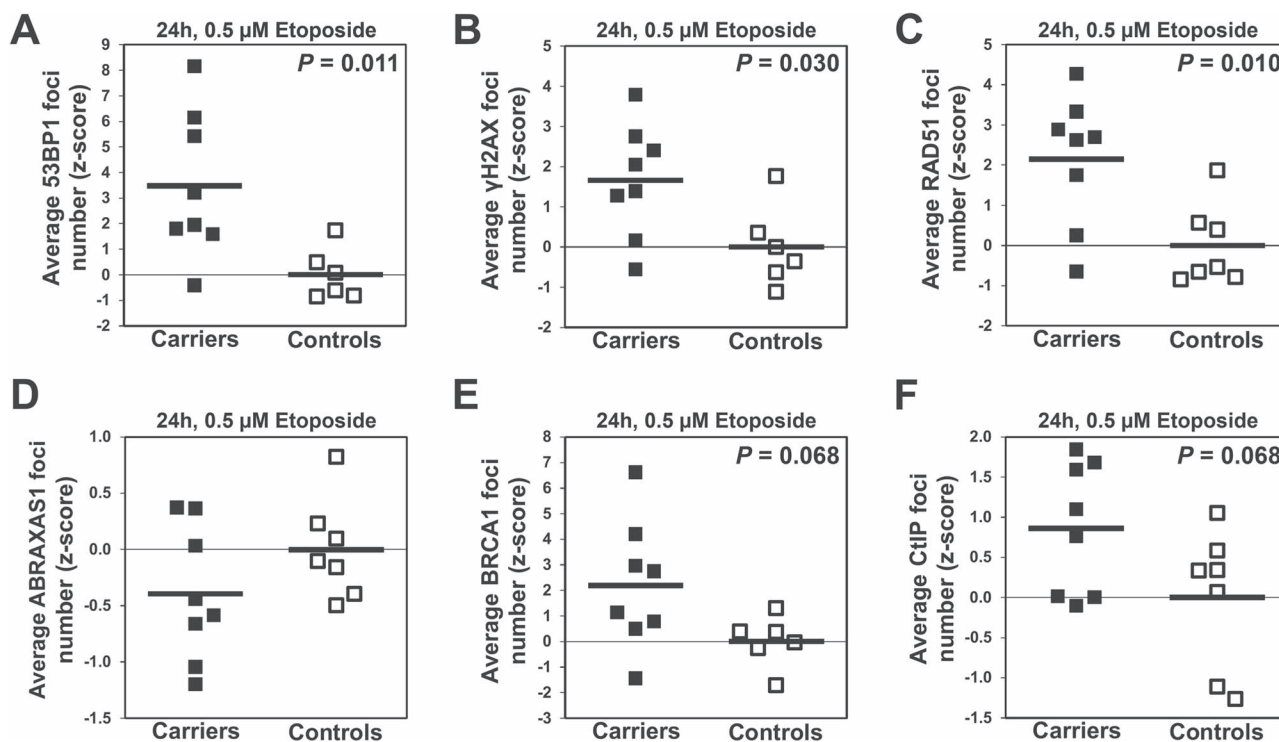


Figure 7. ABRAXAS1 mutation carriers show attenuated DNA damage repair. Foci analysis for 53BP1 (A),  $\gamma$ H2AX (B), RAD51 (C), ABRAXAS1 (D), BRCA1 (E) and CtIP (F) induced after 24 h presence of 0.5  $\mu$ M ETO. Significantly more 53BP1,  $\gamma$ H2AX and RAD51 foci along with comparable ABRAXAS1 foci number and a considerable increase in BRCA1 and CtIP foci was observed in the heterozygous ABRAXAS1 mutation carriers. Lines in the dot plot represent means; statistical significance of differences was evaluated by two-tailed Student's t-test. Dot plot represent results from (A and B) three biological duplicates (BD); >100 nuclei/sample analysed, (C) six BD; >225 nuclei/sample, (D) six BD; >200 nuclei/sample, (E) two BD; >50 nuclei/sample and (F) two BD; >100 nuclei/sample.

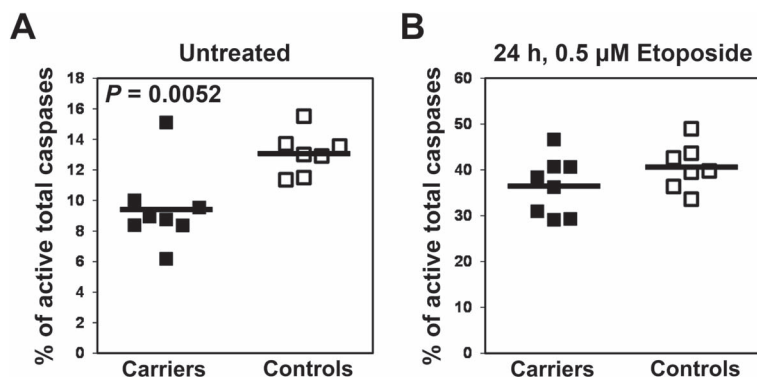


Figure 8. ABRAXAS1 mutation carriers show compromised apoptosis. (A) ABRAXAS1 mutation carriers show a significant decrease in caspase activity during unperturbed growth when compared to controls. (B) There was no difference in caspase activity at 24 h following 0.5  $\mu$ M ETO addition between the cohorts. The fraction of caspase positive cells was determined by flow cytometry after incubation with a fluorescent caspase substrate. Dot plot represent results from two biological duplicates; >60 000 events/sample analysed.

spot' may also explain the observance of the same ABRAXAS1 germline mutation in the NLS domain in different populations not sharing a common geographic and ethnical origin. In addition to BRCA1 and ABRAXAS1, pathogenic variants in genes for other members of the BRCA1-A complex are also implicated in BC (41–43). Thus, as observed for ABRAXAS1 in the current study, we expect to see similar phenotypic changes in cells heterozygous for mutations in genes coding for other BRCA1-A subunits. The phenotype described here not only provides a mechanistic insight on how compromised BRCA1-A function may drive early stage tumorigenesis, but also emphasizes that complex combinations of rather small changes in different key

cellular pathways, such as DNA damage response, DSB repair, DNA replication and cell cycle checkpoint maintenance, may be collectively required to promote tumorigenesis.

## Material and Methods

### Study subjects

Altogether, eight individuals heterozygous for the ABRAXAS1 c.1082G > A founder mutation were analysed in this study. Of these, five individuals had been diagnosed with BC, one with lymphoma and two were disease-free siblings of one BC patient.

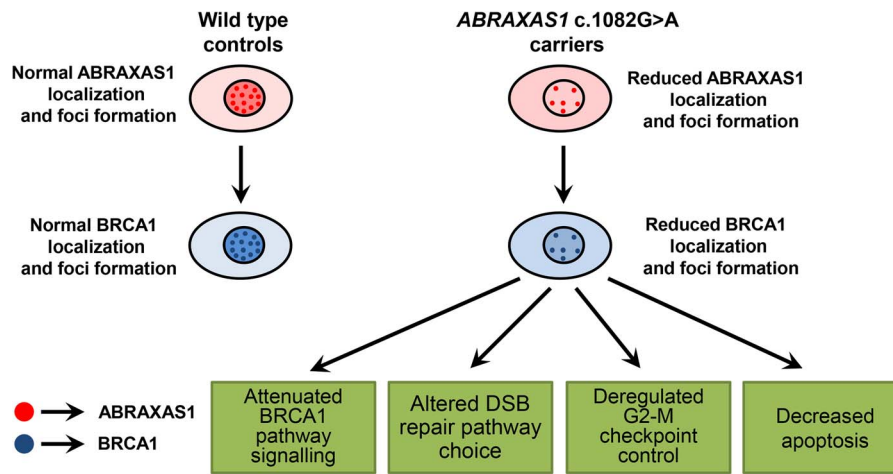


Figure 9. Proposed model for how the heterozygous Finnish ABRAXAS1 c.1082G > A mutation may drive early stage tumorigenesis in carrier individuals. Due to the mutation in the NLS domain, ABRAXAS1 is mislocalized into the cytoplasm that results in reduced ABRAXAS1 nuclear foci formation. Further, a prominent dominant-negative feature of mutant ABRAXAS1 is reduced BRCA1 nuclear foci formation by facilitating BRCA1 mislocalization into the cytoplasm. Reduced BRCA1 localization and foci formation in the carrier cells results in attenuated BRCA1 signalling, altered DSB repair pathway choice, deregulated G2-M checkpoint maintenance and decreased apoptosis. Collectively, changes in the above mentioned pathways likely represent drivers of early stage tumorigenesis in the mutation carriers.

The samples of the BC patients were collected at least 3 years after the initial cancer diagnosis. Seven healthy non-carrier individuals served as controls, one of which is a healthy family member of a patient. For chromosomal analysis, control samples used in a previous study of ours (24) was used again in this study. All controls originated from the same geographical region and had the same ethnical background as the mutation carriers, and were cancer-free at the time of donation. There was no follow-up on the health status of the controls. Informed consent to participate in the study has been obtained from each individual, and the studies have been approved by the Ethical Board of the Northern Ostrobothnia Health Care District and Ethics Committee of the Helsinki University Hospital. Details of the study and control cohort are presented in [Supplementary Material, Table S3](#).

### Cell culture

In order to generate LCLs, Epstein-Barr virus was used to immortalize B-lymphocytes obtained from fresh peripheral blood samples of the participating individuals. LCLs were cultured in RPMI 1640 medium (Gibco/Invitrogen, Carlsbad, CA, U.S.A.) supplemented with 20% fetal bovine serum (Gibco, Invitrogen), 1% L-glutamine (Gibco, Invitrogen) and 10 µg/ml gentamycin (B. Braun Melsungen, Germany). MCF7 BC cell line (ATCC HTB-22™, Manassas, Virginia, USA) was cultured in Dulbecco's modified Eagle Medium, high glucose, with sodium pyruvate (Gibco, Invitrogen) supplemented with 10% fetal bovine serum, 100 IU/ml penicillin and 100 µg/ml streptomycin (Sigma-Aldrich Steinheim, Germany). All cells were maintained at 37°C in a 5% CO<sub>2</sub> atmosphere. All cell lines were tested yearly and were negative for mycoplasma contamination.

### Plasmids and transfection

Wt and c.1082G > A mutant ABRAXAS1 carrying an N-terminal HA/FLAG-tag were cloned from pOZ-N-ABRAXAS1 vectors into pcDNA3.1/Hygro(-) backbone. MCF7 cells were transiently transfected with wt ABRAXAS1, ABRAXAS1 mutant or empty pcDNA3.1/Hygro(-) vector using Cell Line Nucleofector kit V

(Lonza) according to the manufacturer's instructions. Nucleofector program E-014 was used for higher cell viability.

### WB analysis

Cell lines treated with either 5 µM ETO (Etopofos, Bristol-Myer Squibb and/or ETO, Pfizer, Sigma-Aldrich) or 2 mM hydroxyurea (Sigma-Aldrich), were cultured up to 24 h in the presence of the agent. Samples were then collected at different time points (0, 0.5, 1, 2, 3, 5, 7 and 24 h). Following washing, cells were lysed using NETN-300 buffer (20 mM Tris base (pH 7.5), 300 mM NaCl, 1 mM EDTA, 0.5% NP-40, 1× complete mini EDTA protease inhibitor (Roche Diagnostics Mannheim, Germany) and 1× phosphatase inhibitor (Calbiochem Darmstadt, Germany, set V). Cell lysate was then separated using SDS-PAGE (7.5% or 4–15% Mini-PROTEAN TGX precast gels, Bio-Rad Helsinki, Finland) and blotted on to polyvinylidene fluoride (PDVF) membranes. Membranes were blocked with 1% BSA and 1% non-fat dry milk in 1× TBST (50 mM Tris, pH 7.5, 150 mM NaCl, 0.05% Tween 20). Antibody incubations were performed in 1× TBST containing 0.2% BSA and 0.2% non-fat dry milk. The antibodies used in this study are listed in [Supplementary Material, Tables S4 and S5](#). Blots were developed as per the manufacturer's instructions using either SuperSignal™ West Pico Chemiluminescent Substrate or SuperSignal™ West Femto Maximum Sensitivity Substrate (both Thermo Fisher Scientific). Chemiluminescence was detected using Fujifilm LAS-3000 imaging system. Densitometry values were calculated using ImageQuant TL software (GE Healthcare Helsinki, Finland).

### Flow cytometric analysis

Unexposed and 0.5 µM ETO treated cell lines were cultured for 24 h and samples were collected at different time points (0.25, 1, 7 and 24 h). Cells were stained with thymidine analogue 5-ethynyl-2'-deoxyuridine (EdU) to measure DNA synthesis and analyse cell cycle distribution as described by the manufacturer of Click-iT® EdU Alexa Fluor® (AF) 647 Flow Cytometry Assay Kit (Thermo Fisher Scientific, Vantaa, Finland). Cells were fixed with 4% PFA and permeabilized using 0.25% Triton X-100. Blocking

was done with 5% donkey serum. Antibody incubations were performed in TBP buffer (triton X-100 and BSA in PBS) buffer (0.2% Triton X-100 and 1% BSA in PBS). All measurements were performed with LSRFortessa (BD Biosciences Vantaa, Finland) flow cytometer. FlowJo software was used for quantification and the gating strategy used for the analysis is available upon request.

### Immunofluorescence and high content analysis

Immunofluorescence was used to automatically (1) analyse foci number and its characteristics (of  $\gamma$ H2AX, 53BP1, ABRAXAS1, BRCA1, CtIP, RAD51) in the AKLIDES NUK high content analysis system (Medipan Dahlewitz, Germany), and (2) characterize localization patterns of ABRAXAS1, CtIP and BRCA1 between nucleus and cytoplasm using the Operetta high content imaging system (PerkinElmer). For both purposes, untreated cells and cell lines grown in the presence of 0.5  $\mu$ M ETO for up to 24 h were used. Samples were collected at 0, 3, 7 and 24 h. Following washing, LCLs were pipetted on to the slides coated with Teflon and silane (TEKDON Myakka City, Florida, U.S.A.) and MCF7 into black CellCarrier 96-well plates (PerkinElmer Turku, Finland).

Cells were fixed with 2% or 4% PFA and permeabilized using 0.2% Triton X-100. Blocking was done using 5% donkey serum. Antibody incubations were performed either in 1% BSA or in 5% donkey serum—0.3 M glycine—0.05% tween 20. Functionality of the staining procedures were controlled by fluorescence microscopic inspection before subjecting the sample to automated microscopy.

More details on the organization and functioning of both hardware and software component of the automated AKLIDES NUK is explained elsewhere (44,45), exemplary images and the analysis pipeline is presented in [Supplementary Material, Figure S3B](#). In the Operetta high content imaging system, images were acquired and analysed using Harmony PhenoLOGIC 3.5.2 and Columbus 2.5 software, respectively. An exemplary image and the analysis sequence used to find the localization pattern is explained in [Supplementary Material, Figure S2](#) and the analysis script (.aas file) is available upon request.

For both foci and protein localization analysis, different secondary antibody conjugates for the same primary antibody were employed in individual experiments to improve robustness of the analysis. This lead to variation of the absolute values, but not the relative ones, between biological replicates. Therefore, Z-scores were used to report the findings in these cases. The standard formula [ $z = (x - \mu) / \sigma$ ; where  $x$  represents the individual experimental value,  $\mu$  and  $\sigma$  the average and standard deviation of the respective experiment and  $z$  the corresponding z-score] was used to transform the results of individual experiments into z-scores.

### DNA fibre spreads

Exponential growing cells were pulse labelled with 25  $\mu$ M CldU (Sigma) followed by 250  $\mu$ M IdU (Sigma) for the indicated times. For fibre analysis, after damage induction CldU and IdU media was given for indicated time periods and 10  $\mu$ M ETO were performed during the last 30 min of the CldU pulse. Labelled cells were harvested and DNA fibre spreads prepared on microscope glass slides by addition of 200 mM Tris-HCl pH 7.4, 50 mM EDTA, 0.5% SDS (46). Acid-treated fibre spreads were stained with monoclonal rat anti-BrdU followed by monoclonal mouse anti-BrdU. Fibres were examined using fluorescence microscope Axioplan 2 (Zeiss, Germany). CldU and IdU tracks

were measured using ImageJ and micrometre values were converted into kilobases (47). At least 200 replication forks were analysed. Different classes of tracks were classified; red-green (ongoing replication), red (stalled or terminated forks), green (second pulse origin) and red-green-green-red (first pulse origin). Frequencies were calculated using ImageJ software.

### Caspase activation assay

Untreated and cell lines treated with 0.5  $\mu$ M ETO were cultured for 24 h and samples were collected. Further, caspase activation assay was performed using the 660 Polycaspase Assay kit (ImmunoChemistry Technologies, Bloomington, MN, U.S.A.) according to the manufacturer's instruction. All measurements were done in LSRFortessa (BD Biosciences) flow cytometer. FlowJo software was used for quantification and the gating strategy used for the analysis is available upon request.

### Repair pathway analysis

DNA DSB repair was analysed by use of our EGFP-based test system, as described earlier (23,48). In brief, different DNA mixtures, containing expression plasmid for the endonuclease I-SceI (pCMV-I-SceI) together with one of the DSB repair substrates (EJ5SceGFP, EJ-EGFP, 5'EGFP/HR-EGFP, HR-EGFP/3'EGFP, HR-EGFP/5'EGFP) and pBS filler plasmid (pBlueScriptII) or wt EGFP expression plasmid (for determination of transfection efficiencies) were introduced by use of a Gene Pulser with Pulse Controller from Bio-Rad (München, Germany) at 220 V and 1050  $\mu$ F. Subsequently, the cells were recultivated for 48 h and harvested for flow cytometric analysis using FACSCalibur (Becton-Dickinson, Heidelberg, Germany). Recombination frequencies were measured by quantification of green fluorescent cells containing reconstituted EGFP within the life cell-population (SSC/FSC gate) and were individually corrected for transfection efficiencies determined in split samples each. Laser excitation was effected at 488-nm and green fluorescent cells were detected in the FL1/FL2 channel. The recombination frequency was calculated by green fluorescent cells per life cell count divided by the transfection efficiency per life cell count.

### Proximity ligation assay

LCLs were exposed to 2 Gy of ionizing radiation (Cs-137, GSR D1, Gamma-Service Medical GmbH, Leipzig, Germany) and harvested after 4 h. After cytospinning (Cytospin3 Centrifuge, Shandon, Bohemia, NY, USA) at 28  $\times$  g for 5 min on slides covered by poly-L-Lysine (Sigma-Aldrich), cells were fixed immediately with 3.7% formaldehyde followed by permeabilization with 0.5% TritonX-100, washing and blocking steps with 5% goat serum (Invitrogen, Karlsruhe, Germany) in PBS. Then cells were double-stained with the primary antibodies anti-ABRAXAS1 (Abcam, Cambridge, U.K. ab139191) and anti-BRCA1 (Calbiochem, OP92). PLA-stain was then performed using Duolink<sup>®</sup> in Situ Orange Starter Kit Mouse/Rabbit (Sigma, DUO92102). Glass slides were stained with Duolink<sup>®</sup> In Situ PLA<sup>®</sup> Probe Anti-Rabbit PLUS (Sigma, DUO92002) and Duolink<sup>®</sup> In Situ PLA<sup>®</sup> Probe Anti-Mouse MINUS (Sigma, DUO92004) for 1 h at 37°C. After washing the samples were incubated with the ligation–ligase reaction solution for 30 min at 37°C to hybridize oligonucleotides tagged on probes. After two short washing steps, the glass slides were incubated with the amplification–polymerase reaction solution for 100 min at 37°C to amplify hybridized oligonucleotides and fluorescently label the amplification products. Then, glass slides were cov-

ered with coverslips using Duolink® In Situ Mounting Medium with DAPI (Sigma, DUO82040). Imaging was performed using Keyence BZ-9000 microscope (Keyence Neu-Isenburg, Germany). Automated quantification of PLA-foci was carried out with BZ-II Analyser software.

### Chromosomal analysis

Chromosomal analysis of four heterozygous ABRAXAS1 c.1082G > A carriers (one healthy carrier, three carriers diagnosed with BC) and nine controls was carried out on metaphases obtained from regular short-term 3-day cultures of peripheral blood T-lymphocytes. The blood samples of the studied BC patients ( $n = 3$ ) were collected 4–18 years after the initial cancer diagnosis. A minimum of 50 Giemsa-banded metaphases for each sample were evaluated as mentioned (24).

### Statistical analysis

Statistical differences for normally and non-normally distributed samples were determined using independent samples student's *t*-test and Mann–Whitney *U*-test, respectively. Mean values are reported for normally distributed samples; in case of non-normally distributed samples, median values are reported. Correlation analysis was done using Spearman's rank correlation coefficient and rho scores were reported. All *P*-values were two-sided and statistical evaluations were done with IBM SPSS Statistics (version 20.0).

The statistical significances of PLA foci analyses were determined by the GraphPad Prism 5.04 software (GraphPad, San Diego, CA, USA) using non-parametric Mann–Whitney test for unpaired samples. Cohort analyses of DSB repair pathway usage were performed using IBM SPSS Statistics Software package version 21. DSB repair pathway usage was analysed using a general linear mixed model with mutation as fixed factor and date of experiment as random factor.

### Supplementary Material

Supplementary Material is available at HMG online.

### Author Contributions

H.Po. and R.W. conceived, designed and oversaw the study with helpful input from L.W. and K.B. The R.W. lab was responsible for collecting suitable blood samples from ABRAXAS1 mutation carriers and controls for the generation of LCLs and chromosomal analysis. H.N. provided some additional ABRAXAS1 mutation carrier blood samples. M.B. performed the WB analyses, qPCR, flow cytometry analyses, protein localization analysis, DNA damage signalling PCR array, caspase activation assay and the foci analysis with assistance from L.H., F.M., and H.Pe. N.L. performed the MCF7 experiments. H.T. cloned the vectors used for MCF7 experiments. A.P., J.W. and K.B. carried out the DNA fibre assay studies. J.S. carried out repair pathway analysis, RPA foci analysis and PLA. J.J. performed AlamarBlue assays. K.P. together with K.R. were responsible for the cytogenetic analysis. M.G. performed RNA-Seq. Statistical analyses were done with technical assistance from P.N. and T.F. M.B. drafted the manuscript, R.W. and H.Po. prepared the final manuscript, all authors contributed to critical review of the paper.

### Conflict of Interest

L.H. has been employee of Medipan, the company marketing the Aklides NUK high content analysis platform used for foci analysis. L.W. is inventor and patent owner of a test system for determining genotoxicities.

### Funding

Academy of Finland (Grant number 122715 and Center of Excellence Grant number 251314), the Finnish Cancer Foundation, the Sigrid Jusélius Foundation, the Cancer Fund of Northern Finland, the University of Oulu, the University of Oulu Support Foundation, the University of Oulu Graduate School, the Oulu University Hospital, the Orion-Farmos Research Foundation, the Ida Montin Foundation, K. Albin Johansson Foundation, the German Federal Office for Radiation Protection (UFA Grant 3610S30016), the German Federal Ministry of Education and Research (BMBF Grants 02NUK032 and 02NUK035B), the Hamburger Krebsgesellschaft e.V. and the International Graduate School in Molecular Medicine Ulm, Germany. The Fritz Lipmann Institute is a member of the Science Association 'Gottfried Wilhelm Leibniz' (WGL) and financially supported by the Federal Government of Germany and the State of Thuringia.

### Acknowledgements

We thank V. Glumoff, I. Goerlich, V. Jennifer, L. Kesitalo, K. Mononen, M. Otsukka, A. Vääntänen, A. Zielinski, L. Pelttari, J. Kiiski, A. Gleiche and the Laboratory of Genetics at NordLab Oulu for their help. We also thank all patients and their family members for volunteering to participate in this study.

### References

- Castillo, A., Paul, A., Sun, B., Huang, T.H., Wang, Y., Yazinski, S.A., Tyler, J., Li, L., You, M.J., Zou, L. et al. (2014) The BRCA1-interacting protein Abraxas is required for genomic stability and tumor suppression. *Cell Rep.*, **8**, 807–817.
- Wang, B., Matsuoka, S., Ballif, B.A., Zhang, D., Smogorzewska, A., Giyi, S. and Elledge, S.J. (2007) Abraxas and Rap80 form a novel BRCA1 protein complex required for the DNA damage response. *Science*, **316**, 1194–1198.
- Kim, H., Huang, J. and Chen, J. (2007) CCDC98 is a BRCA1-BRCT domain-binding protein involved in the DNA damage response. *Nat. Struct. Mol. Biol.*, **14**, 710–715.
- Liu, Z., Wu, J. and Yu, X. (2007) CCDC98 targets BRCA1 to DNA damage sites. *Nat. Struct. Mol. Biol.*, **14**, 716–720.
- Kyrieleis, O.J.P., McIntosh, P.B., Webb, S.R., Calder, L.J., Lloyd, J., Patel, N.A., Martin, S.R., Robinson, C.V., Rosenthal, P.B. and Smerdon, S.J. (2016) Three-dimensional architecture of the human BRCA1-a histone deubiquitinase core complex. *Cell Rep.*, **17**, 3099–3106.
- Solyom, S., Aressy, B., Pylkäs, K., Patterson-Fortin, J., Hartikainen, J.M., Kallioniemi, A., Kauppila, S., Nikkilä, J., Kosma, V.-M., Mannermaa, A. et al. (2012) Breast cancer-associated Abraxas mutation disrupts nuclear localization and DNA damage response functions. *Sci. Transl. Med.*, **4**, 122ra23.
- Brown, J.S. and Jackson, S.P. (2015) Ubiquitylation, neddylation and the DNA damage response. *Open Biol.*, **5**, 150018–150018.

8. Hu, Y., Scully, R., Sobhian, B., Xie, A., Shestakova, E. and Livingston, D.M. (2011) RAP80-directed tuning of BRCA1 homologous recombination function at ionizing radiation-induced nuclear foci. *Genes Dev.*, **25**, 685–700.
9. Shao, G., Patterson-Fortin, J., Messick, T.E., Feng, D., Shanbhag, N., Wang, Y. and Greenberg, R.A. (2009) MERIT40 controls BRCA1–Rap80 complex integrity and recruitment to DNA double-strand breaks. *Genes Dev.*, **23**, 740–754.
10. Feng, L., Wang, J. and Chen, J. (2010) The Lys 63-specific deubiquitinating enzyme BRCC36 is regulated by two scaffold proteins localizing in different subcellular compartments. *J. Biol. Chem.*, **285**, 30982–30988.
11. Kim, H., Chen, J. and Yu, X. (2007) Ubiquitin-binding protein RAP80 mediates BRCA1-dependent DNA damage response. *Science*, **316**, 1202–1205.
12. Sobhian, B., Shao, G., Lilli, D.R., Culhane, A.C., Moreau, L.A., Xia, B., Livingston, D.M. and Greenberg, R.A. (2007) RAP80 targets BRCA1 to specific ubiquitin structures at DNA damage sites. *Science*, **316**, 1198–1202.
13. Feng, L., Huang, J. and Chen, J. (2009) MERIT40 facilitates BRCA1 localization and DNA damage repair. *Genes Dev.*, **23**, 719–728.
14. Wang, B. and Elledge, S.J. (2007) Ubc 13/Rnf 8 ubiquitin ligases control foci formation of the Rap80/Abraxas/Brcr 1/Brcr 36 complex in response to DNA damage. *Proc. Natl. Acad. Sci.*, **104**, 20759–20763.
15. Wang, B. (2012) BRCA1 tumor suppressor network: focusing on its tail. *Cell Biosci.*, **2**, 6.
16. Draga, M., Madgett, E., Vandenberg, C., du Plessis, D., Kaufmann, A., Werler, P., Chakraborty, P., Lowndes, N. and Hiom, K. (2015) BRCA1 is required for maintenance of phospho-Chk 1 and G2/M arrest during DNA crosslink repair in DT40 cells. *Mol. Cell. Biol.*, **35**, 3829–3840.
17. Lek, M., Karczewski, K.J., Minikel, E.V., Samocha, K.E., Banks, E., Fennell, T., O'Donnell-Luria, A.H., Ware, J.S., Hill, A.J., Cummings, B.B. et al. (2016) Analysis of protein-coding genetic variation in 60,706 humans. *Nature*, **536**, 285–291.
18. Vikrant Kumar, R., Siddiqui, Q., Singh, N., Waghmare, S.K. and Varma, A.K. (2015) Mislocalization of BRCA1-complex due to ABRAXAS Arg 361Gln mutation. *J. Biomol. Struct. Dyn.*, **33**, 1291–1301.
19. Bennardo, N., Cheng, A., Huang, N. and Stark, J.M. (2008) Alternative-NHEJ is a mechanistically distinct pathway of mammalian chromosome break repair. *PLoS Genet.*, **4**, e1000110.
20. Pathania, S., Bade, S., Le Guillou, M., Burke, K., Reed, R., Bowman-Colin, C., Su, Y., Ting, D.T., Polyak, K., Richardson, A.L. et al. (2014) BRCA1 haploinsufficiency for replication stress suppression in primary cells. *Nat. Commun.*, **5**, 5496.
21. Polato, F., Callen, E., Wong, N., Faryabi, R., Bunting, S., Chen, H.-T., Kozak, M., Kruhlak, M.J., Reczek, C.R., Lee, W.-H. et al. (2014) CtIP-mediated resection is essential for viability and can operate independently of BRCA1. *J. Exp. Med.*, **211**, 1027–1036.
22. Keimling, M., Deniz, M., Varga, D., Stahl, A., Schrezenmeier, H., Kreienberg, R., Hoffmann, I., König, J. and Wiesmüller, L. (2012) The power of DNA double-strand break (DSB) repair testing to predict breast cancer susceptibility. *FASEB J.*, **26**, 2094–2104.
23. Obermeier, K., Sachsenweger, J., Friedl, T.W.P., Pospiech, H., Winqvist, R. and Wiesmüller, L. (2016) Heterozygous PALB2 c.1592delT mutation channels DNA double-strand break repair into error-prone pathways in breast cancer patients. *Oncogene*, **35**, 3796–3806.
24. Nikkilä, J., Parplys, A.C., Pylkäs, K., Bose, M., Huo, Y., Borgmann, K., Rapakko, K., Nieminen, P., Xia, B., Pospiech, H. et al. (2013) Heterozygous mutations in PALB2 cause DNA replication and damage response defects. *Nat. Commun.*, **4**, 2578.
25. Macheret, M. and Halazonetis, T.D. (2015) DNA replication stress as a hallmark of cancer. *Annu. Rev. Pathol.*, **10**, 425–448.
26. Schoonen, P.M., Guerrero Llobet, S. and van Vugt, M.A.T.M. (2019) Replication stress: driver and therapeutic target in genomically unstable cancers. *Adv. Protein Chem. Struct. Biol.*, **115**, 157–201.
27. Schlacher, K., Wu, H. and Jasin, M. (2012) A distinct replication fork protection pathway connects Fanconi anemia tumor suppressors to RAD51-BRCA1/2. *Cancer Cell*, **22**, 106–116.
28. Choi, S., Gamper, A.M., White, J.S. and Bakkenist, C.J. (2010) Inhibition of ATM kinase activity does not phenocopy ATM protein disruption: implications for the clinical utility of ATM kinase inhibitors. *Cell Cycle*, **9**, 4052–4057.
29. Daniel, J.A., Pellegrini, M., Lee, B.-S., Guo, Z., Filsuf, D., Belkina, N.V., You, Z., Paull, T.T., Sleckman, B.P., Feigenbaum, L. et al. (2012) Loss of ATM kinase activity leads to embryonic lethality in mice. *J. Cell Biol.*, **198**, 295–304.
30. Vaclová, T., Gómez-López, G., Setién, F., Bueno, J.M.G., Macías, J.A., Barroso, A., Urioste, M., Esteller, M., Benítez, J. and Osorio, A. (2015) DNA repair capacity is impaired in healthy BRCA1 heterozygous mutation carriers. *Breast Cancer Res. Treat.*, **152**, 271–282.
31. Lam, M.H., Liu, Q., Elledge, S.J. and Rosen, J.M. (2004) Chk 1 is haploinsufficient for multiple functions critical to tumor suppression. *Cancer Cell*, **6**, 45–59.
32. Sedic, M., Skibinski, A., Brown, N., Gallardo, M., Mulligan, P., Martinez, P., Keller, P.J., Glover, E., Richardson, A.L., Cowan, J. et al. (2015) Haploinsufficiency for BRCA1 leads to cell-type-specific genomic instability and premature senescence. *Nat. Commun.*, **6**, 7505.
33. O'Driscoll, M., Dobyns, W.B., van Hagen, J.M. and Jeggo, P.A. (2007) Cellular and clinical impact of haploinsufficiency for genes involved in ATR signaling. *Am. J. Hum. Genet.*, **81**, 77–86.
34. Hamdi, Y., Soucy, P., Adoue, V., Michailidou, K., Canisius, S., Lemaçon, A., Droit, A., Andrulis, I.L., Anton-Culver, H., Arndt, V. et al. (2016) Association of breast cancer risk with genetic variants showing differential allelic expression: identification of a novel breast cancer susceptibility locus at 4q21. *Oncotarget*, **7**, 49.
35. Pennington, K.P., Walsh, T., Harrell, M.I., Lee, M.K., Pennil, C.C., Rendi, M.H., Thornton, A., Norquist, B.M., Casadei, S., Nord, A.S. et al. (2014) Germline and somatic mutations in homologous recombination genes predict platinum response and survival in ovarian, fallopian tube, and peritoneal carcinomas. *Amer. Assoc. Cancer Res.*, **20**, 764–775.
36. McKay, J.D., Truong, T., Gaborieau, V., Chabrier, A., Chuang, S.-C., Byrnes, G., Zaridze, D., Shagina, O., Szeszenia-Dabrowska, N., Lissowska, J. et al. (2011) A genome-wide association study of upper Aerodigestive tract cancers conducted within the INHANCE consortium. *PLoS Genet.*, **7**, e1001333.
37. Erkkö, H., Xia, B., Nikkilä, J., Schleutker, J., Syrjäkoski, K., Mannermaa, A., Kallioniemi, A., Pylkäs, K., Karppinen, S.-M., Rapakko, K. et al. (2007) A recurrent mutation in PALB2 in Finnish cancer families. *Nature*, **446**, 316–319.
38. Sarantaus, L., Huusko, P., Eerola, H., Launonen, V., Vehmanen, P., Rapakko, K., Gillanders, E., Syrjäkoski, K., Kainu, T., Vahteristo, P. et al. (2000) Multiple founder effects and geographical

- clustering of BRCA1 and BRCA2 families in Finland. *Eur. J. Hum. Genet.*, **8**, 757–763.
39. Dohrn, L., Salles, D., Siehler, S.Y.Y., Kaufmann, J. and Wiesmüller, L. (2012) BRCA1-mediated repression of mutagenic end-joining of DNA double-strand breaks requires complex formation with BACH1. *Biochem. J.*, **441**, 919–926.
  40. Shuen, A.Y. and Foulkes, W.D. (2011) Inherited mutations in breast cancer genes—risk and response. *J. Mammary Gland Biol. Neoplasia*, **16**, 3–15.
  41. Nikkilä, J., Coleman, K.A., Morrissey, D., Pylkäs, K., Erkko, H., Messick, T.E., Karppinen, S.-M., Amelina, A., Winqvist, R. and Greenberg, R.A. (2009) Familial breast cancer screening reveals an alteration in the RAP80 UIM domain that impairs DNA damage response function. *Oncogene*, **28**, 1843–1852.
  42. Antoniou, A.C., Wang, X., Fredericksen, Z.S., McGuffog, L., Tarrell, R., Sinilnikova, O.M., Healey, S., Morrison, J., Kartsonaki, C., Lesnick, T. et al. (2010) A locus on 19p13 modifies risk of breast cancer in BRCA1 mutation carriers and is associated with hormone receptor-negative breast cancer in the general population. *Nat. Genet.*, **42**, 885–892.
  43. Bolton, K.L., Tyrer, J., Song, H., Ramus, S.J., Notaridou, M., Jones, C., Sher, T., Gentry-Maharaj, A., Wozniak, E., Tsai, Y.-Y. et al. (2010) Common variants at 19p13 are associated with susceptibility to ovarian cancer. *Nat. Genet.*, **42**, 880–884.
  44. Willitzki, A., Hiemann, R., Peters, V., Sack, U., Schierack, P., Rödiger, S., Anderer, U., Conrad, K., Bogdanos, D.P., Reinhold, D. et al. (2012) New platform technology for comprehensive serological diagnostics of autoimmune diseases. *Clin. Dev. Immunol.*, **2012**, 284740.
  45. Willitzki, A., Lorenz, S., Hiemann, R., Guttek, K., Goihl, A., Hartig, R., Conrad, K., Feist, E., Sack, U., Schierack, P. et al. (2013) Fully automated analysis of chemically induced  $\gamma$ H2AX foci in human peripheral blood mononuclear cells by indirect immunofluorescence. *Cytometry A*, **83**, 1017–1026.
  46. Parpys, A.C., Petermann, E., Petersen, C., Dikomey, E. and Borgmann, K. (2012) DNA damage by X-rays and their impact on replication processes. *Radiother. Oncol.*, **102**, 466–471.
  47. Jackson, D.A. and Pombo, A. (1998) Replicon clusters are stable units of chromosome structure: evidence that nuclear organization contributes to the efficient activation and propagation of S phase in human cells. *J. Cell Biol.*, **140**, 1285–1295.
  48. Akyüz, N., Boehden, G.S., Süsse, S., Rimek, A., Preuss, U., Scheidtmann, K.-H. and Wiesmüller, L. (2002) DNA substrate dependence of p 53-mediated regulation of double-Strand break repair. *Mol. Cell. Biol.*, **22**, 6306–6317.